



Warzok, F., Allegri, G., Gude, M., & Hallett, S. R. (2016). Experimental Characterisation of Fatigue Damage in Single Z-pins. *Composites Part A: Applied Science and Manufacturing*. DOI: 10.1016/j.compositesa.2016.03.023

Peer reviewed version

License (if available):  
CC BY

Link to published version (if available):  
[10.1016/j.compositesa.2016.03.023](https://doi.org/10.1016/j.compositesa.2016.03.023)

[Link to publication record in Explore Bristol Research](#)  
PDF-document

This is the author accepted manuscript (AAM). The final published version (version of record) is available online via Elsevier at <http://www.sciencedirect.com/science/article/pii/S1359835X16300409>. Please refer to any applicable terms of use of the publisher.

## **University of Bristol - Explore Bristol Research**

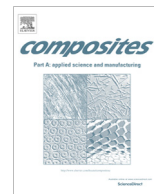
### **General rights**

This document is made available in accordance with publisher policies. Please cite only the published version using the reference above. Full terms of use are available:  
<http://www.bristol.ac.uk/pure/about/ebr-terms.html>



Contents lists available at ScienceDirect

## Composites: Part A

journal homepage: [www.elsevier.com/locate/compositesa](http://www.elsevier.com/locate/compositesa)

## Experimental characterisation of fatigue damage in single Z-pins

F. Warzok<sup>a,b,\*</sup>, G. Allegri<sup>a</sup>, M. Gude<sup>b</sup>, S.R. Hallett<sup>a</sup><sup>a</sup> Advanced Composite Centre for Innovation and Science (ACCIS), University of Bristol, Queen's Building, University Walk, BS8 1TR, UK<sup>b</sup> Institute of Lightweight Engineering and Polymer Technology (ILK), Technische Universität Dresden, Holbeinstr. 3, 01307 Dresden, Germany

## ARTICLE INFO

## Article history:

Received 22 July 2015

Received in revised form 5 February 2016

Accepted 23 March 2016

Available online xxxx

## Keywords:

A. 3-Dimensional reinforcement

B. Wear

C. Fatigue

D. Microstructural analysis

## ABSTRACT

Z-pins have been shown to significantly improve delamination resistance and impact strength of carbon fibre reinforced (CFRP) composites. In this paper, an experimental investigation of the influence of different fatigue parameters (mean opening/sliding displacement, amplitude, frequency, number of cycles) on the through-thickness reinforcement (TTR) is presented. For mode I, it is shown that the degradation on pin behaviour during fatigue is mostly affected by the applied displacement amplitude. The degradation is primarily caused by surface wear. Due to the brittleness of the Z-pins, mode II fatigue does not have a significant effect for very small sliding displacements. Exceeding a critical displacement causes the pin to rupture within the very first cycles.

© 2016 The Authors. Published by Elsevier Ltd. This is an open access article under the CC BY license (<http://creativecommons.org/licenses/by/4.0/>).

## 1. Introduction

Due to their excellent specific mechanical properties, which combine high strength, high stiffness and low density, carbon fibre reinforced plastics are becoming widely used for the development and design of lightweight structures. In aviation, both Airbus (A350 XWB) and Boeing (B787 Dreamliner) have introduced aircraft for which carbon fibre laminates constitute 50% of the overall structural weight [1,2]. However, due to their layered structure, CFRP exhibit low through-thickness properties and can be prone to delaminate. The resulting interlaminar cracks cause a reduction of impact resistance [3,4] and fatigue life [5,6].

In order to overcome these disadvantages, discrete reinforcements [7–9] can be applied to composites in the through-thickness direction. However, many of these technologies lead to excessive damage during the introduction of the reinforcements. Z-pinning is one of the very few technologies that is applicable to prepregs. It utilises small high stiffness and/or high strength rods which are inserted into a laminate before curing [10].

Although it has been shown that the initiation of cracks cannot be prevented by Z-pins [11–16], delamination growth is successfully inhibited in laminates and bonded joints in mode I [10,11,15–21], mode II [10,11,18,19,22–24] and mixed mode I/II [10,18,21,25]. The toughness enhancement provided by Z-pinning

is influenced by various design parameters such as pin diameter, pin shape, pin or laminate material [4,26,27].

Recently, the fatigue behaviour of Z-pinned composites has attracted research interest. In a micro-mechanical study, Zhang et al. [28] performed cyclic mode I tests on five-harness satin carbon/epoxy prepreg specimens reinforced with a Z-pin array. Two displacement-controlled fatigue scenarios were considered: the first was based on cycling the displacement before reaching the peak static pull-out load  $P$  – in the second scenario a cyclic displacement was applied in the frictional pull-out region. Quasi-static tests were performed to assess the displacement at  $P$ ,  $\delta_p$ . In the publication  $P$  is considered to be the Z-pin debonding load, as it is followed by a sudden drop. However,  $\delta_p$  was measured to be  $\sim 0.45$  mm for large  $\varnothing 0.51$  mm pins and  $\sim 0.35$  mm for small  $\varnothing 0.28$  mm pins. For the 3 mm thick specimens employed, this results in a failure strain  $\epsilon_f = 15\%$  and  $\epsilon_f = 12\%$ . However,  $\epsilon_f$  of the neat resin is 1.5% [29]. To assess the degradation of  $P$ , residual pull-out tests were performed after cyclic loading. In the first case an ongoing decrease of  $P$  was found after increasing number of cycles. The degradation became substantially larger after  $10^3$  cycles and was more pronounced for the larger pins. Even though, further pull-out did not show an obvious decrease of the frictional loads. For the second scenarios the loads were recorded at certain cycles and compared to the initial load. Again, degradation considerably accelerated after  $10^3$  cycles. SEM pictures show that the laminate surface had been worn out during the fatigue tests by microcracking of the resin.

Cartié et al. [19] presented the first coupon-level study on the fatigue properties of Z-pinned DCB and ELS specimens. Due to

\* Corresponding author at: Advanced Composite Centre for Innovation and Science (ACCIS), University of Bristol, Queen's Building, University Walk, BS8 1TR, UK.

E-mail address: [felix.warzok@bris.ac.uk](mailto:felix.warzok@bris.ac.uk) (F. Warzok).

heavily misaligned pins, load controlled fatigue was applied to the TT reinforced specimens, while displacement controlled fatigue was applied to the unpinned reference coupons. It was shown that for both mode I and II the pins significantly slow down the crack propagation during fatigue loading, as long as a threshold limit that causes complete pin pull-out is not exceeded. However, a significant change in pin failure between quasi-static and fatigue testing was reported. While the pins pulled out completely in the former case, pin rupture at a very small pull-out displacement was observed in the latter.

Pegorin et al. [30] presented an experimental study on the fatigue properties of pinned DCB and ENF coupons. In order to assess the fatigue strength, the amplitude  $\Delta\delta$  and thus the interlaminar strain energy release rate  $G$  was increased during testing. Increasing the Z-pin density raised the fatigue delamination onset stress, as well as the critical  $G$  that corresponded to unstable crack propagation. At the same time, delamination propagated at a slower rate (as in [19]). Pins were more effective in mode I than in mode II. No effect of the applied amplitude could be discerned. In contrast to [19], complete pin pull-out was observed in mode I fatigue.

So far the only study on the degradation of the TTR itself has been presented by Zhang et al. [28] focussing on mode I and considering rather small displacements. With regard to the studies on the crack growth speed, it would be important to establish whether similar results could be observed if  $\Delta G$  was decreased instead of increased during testing or whether a change in crack propagation could be observed if  $\Delta G$  was kept constant for a sufficiently long time. Finally, Zhang et al. [28] did not comment on energy dissipation during fatigue cycling, which might help to predict crack growth in pinned laminates.

Despite the enhancements reported for quasi-static loading, the limited amount of research done on the in-service performance of Z-pinned structures may hamper more widespread application. The goal of this study is to improve the understanding of the fatigue performance of carbon Z-pins to help assessing their benefit for certain applications. The influence of average displacement  $\delta_0$ , amplitude  $\Delta\delta$ , frequency  $f$  and fracture mode is investigated. As in [26], single pin specimens were tested to isolate and understand the pin fatigue behaviour. Non-fatigue related effects like load redistribution in a multi pin array may conceal fatigue performance. Previous studies on fatigue behaviour in Z-pinned laminates have shown relatively high amounts of scatter in testing [26]. Using one pin per specimen facilitates better tracking of variability. Finally, the single pin testing also allows for more consistent mode II testing conditions, as the whole specimen can easily be loaded with or against the pin inclination (Section 3). Transfer of the findings into analytical and numerical models will be the subject of future work, to facilitate the design process.

## 2. Specimen manufacture

The manufacture of the single Z-pin specimens followed the procedure outlined in [26], where a comprehensive study on quasi-static Z-pin properties was conducted. A schematic view of the specimens is shown in Fig. 1. The relatively thick laminate

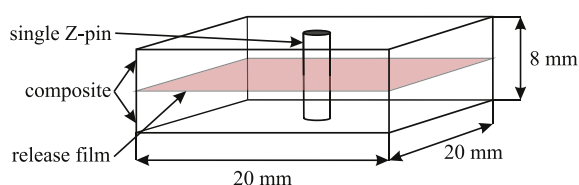


Fig. 1. Single Z-pin specimen. (For interpretation of the references to colour in this figure legend, the reader is referred to the web version of this article.)

allows considering a variety of combinations of  $\delta_0$  and  $\Delta\delta$  in the mode I fatigue test. However, a very stiff foundation of the pins is provided, thus limiting rotation and sliding in mode II [27]. Toral Vazquez et al. [31] undertook single Z-pin testing embedding the pin into pure resin. However, as the shape of the resin pocket and thus the pin-laminate interface is affected by the stacking sequence [26], the use of composite specimens is more representative of real structures. The laminate is manufactured using the following specifications:

- IM7/8552 prepreg (Hexcel, UK)
- 64 0.125 mm thick plies, for a total thickness of 8 mm
- Zero-dominated (ZD) layup with two symmetric sublaminaes
  - Stacking sequence:  $[(45/0/-45/0)_{4s}/*(-45/0/45/0)_{4s}]$
  - 0.016 mm FEP fluoropolymer film in midplane (\*)

In order to prevent interpenetration and thus interlocking of the prepreg fibres, a nonsymmetric stacking sequence with a 90° orientation change at the midplane is utilised. Inserting the FEP film ensures that only the individual pin response is measured in the experiments.

T300 carbon/BMI Ø0.28 mm Z-pins are employed as TTR. In order to reduce misalignment, the pins are inserted directly into a heated laminate. Silicone rubber plates are placed between the laminate and the caul plates during autoclaving, as the use of metallic plates only has been identified as a further source of pin misalignment [19]. Using the manufacturing method described above the Z-pin misalignment is reduced to an average of 5°. After curing, 20 mm by 20 mm specimens are cut from the composite plate. Because of the rubber plates small pin protrusions are visible after curing on both sides of the composite. These are ground down to ensure a proper specimen positioning during testing.

## 3. Experimental testing

Single Z-pin tests were conducted on servo-hydraulic Instron 8872 25 kN and Instron MJ 6272 machines. Calibrated 1 kN load cells have been used on a 25 kN load frame. For the fatigue tests these were attached to the static side to remove possible inertia effects. Instron hydraulic wedge grips were used for both mode I and mode II testing. Aluminium lightweight load fixtures have been designed for fatigue testing (Fig. 2). The mode II rig specimen recess is tilted by 3° to prevent any frictional forces between the two laminate interfaces at the midplane, which would conceal the measurement of the Z-pin forces. As the pins have shown an average misalignment of 5° it was still possible to test a very high mode mix. However, pure mode II is not possible for this configuration as for this to be achieved the two halves of the fixture would need to be at zero degrees (parallel to the loading direction) and constrained from lateral movement to prevent any form of crack opening. It is hence denoted as “mode II”. Due to the tilted specimen recess no alternating fatigue loads can be tested. The rig has been designed in such way that specimens can be fatigued in “mode II” with subsequent mode I pull out.

For mode I fatigue testing the specimen is glued onto the bottom rig first. After applying some glue on the specimen top, the testing machine is closed and a low pressure force (ca. –30 N) is held for 5 min. Subsequently the grips are carefully separated until the pressure load is reduced to zero. The test is then started. For “mode II” the specimen is glued into one of the two similar rigs, which is then gripped by the testing machine. Inside the testing machine the other rig is carefully pushed against the specimen and the grips are closed. In the next step small portions of glue are put on the specimen edges, which get then drawn into the gap between rig and specimen by capillary action. After the glue

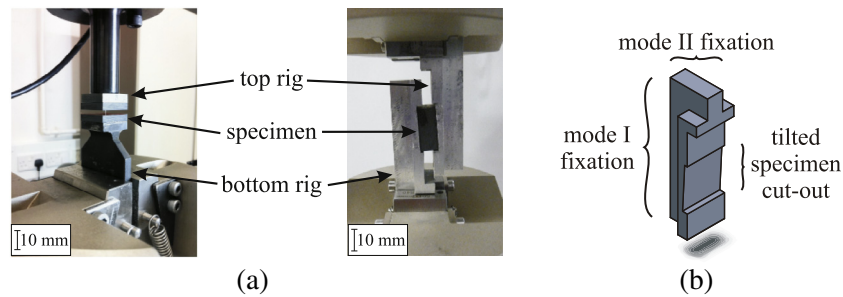


**Fig. 2.** (a) Mode I (left) and mode II (right) rig during testing and (b) sketch of the mode II rig. (For interpretation of the references to colour in this figure legend, the reader is referred to the web version of this article.)

**Table 1**  
Overview of the displacement controlled fatigue tests.

Denotation	$f$ (Hz)	$\delta_0$ (mm)	$\Delta\delta$ (mm)	$n$	Tests
<i>Mode I fatigue</i>					
$F_I-1$	2; 5	0.15	0.05	$10^5$	5
$F_I-1-1$	5	0.15	0.05	$10^6$	5
$F_I-2$	2; 5	1.5	0.8	$10^5$	5
$F_I-2-1$	5	1.5	0.8	$10^6$	5
$F_I-3$	2; 5	3	0.05	$10^5$	5
$F_I-4$	2; 5	3	0.8	$10^5$	5
<i>Mode II fatigue</i>					
$F_{II}-1$	2; 5	0.1	0.05	$10^5$	7
$F_{II}-1-1$	2	0.1	0.05	$5 \times 10^5$	5
$F_{II}-2$	2; 5	0.15	0.05	$10^5$	16
$F_{II}-2-1$	2; 5	0.15	0.05	$5 \times 10^5$	10
$F_{II}-3$	5	0.2	0.05	$10^5$	3

has been left to dry for 5 min the test is started. Cyanoacrylate glue is used for all tests.

All fatigue tests were undertaken in displacement control. After an initial  $\delta_0$  was reached quasi-statically (0.25 mm/min), the specimen was fatigued with  $\Delta\delta$  and  $f$  for a given number of cycles  $n$ . The full range  $\Delta\delta$  was built up over 10 cycles (small  $\Delta\delta$ ) and 300 cycles (large  $\Delta\delta$ ), respectively. Subsequently the quasi-static test was continued until final failure. An overview of the tested fatigue regimes is given in Table 1. Quasi-static tests without fatigue loading were also carried out in order to quantify the effect of cyclic loading.

The frequencies and displacements used in this testing programme resulted in a displacement rate range of 0.005–0.08 m/s.

Preliminary testing of single Z-pin specimens at increased loading rates (0.1 m/s and 0.3 m/s) was undertaken to quantify the accuracy of the test machine cross head displacement measurements. A high speed camera was used to take optical measurements for comparison. The camera resolution was set to  $384 \times 416$  pixels and 30,000 frames per second were used. Correlation between both measurements was consistent and considered good enough so as not to require additional optical instruments for the fatigue testing.

Fig. 3 illustrates the various fatigue displacement ranges considered, overlaid with the static response of a single pin specimen. Suitable ranges were chosen to represent possible in service-conditions. Vibration-like behaviour with very small  $\Delta\delta$  was considered before ( $F_I-1$ ) and after ( $F_I-3$ ) significant crack opening. Additionally large  $\Delta\delta$  after major crack growth were considered to represent fatigue in a damaged, more compliant structure ( $F_I-2$  and  $F_I-4$ ). To quantify the effect of  $\delta_0$  two configurations were chosen. Since safety-relevant structures may need to be in service even after cracks are apparent two configurations ( $F_I-1-1$  and  $F_I-2-1$ ) with higher  $n$  were tested. None of these regimes causes a complete pull-out of the pin. Due to pin misalignment, it is highly unlikely that a pin will re-enter the laminate once pulled out. At least 5 specimens have been tested per configuration. To confirm results a higher number has been chosen for some of the “mode II” configurations.

The “mode II” tests were conducted so that the specimens were loaded against pin inclination (Fig. 4) to prevent any form of mode I loading. This allows applying only very small displacements before final failure. The effect is enhanced by the relatively thick specimens, which provide a very stiff pin foundation and prevent significant pin bending [27]. Thus, only vibration-like behaviour could be investigated in which  $\delta_0$  and  $n$  were varied to quantify their influences.

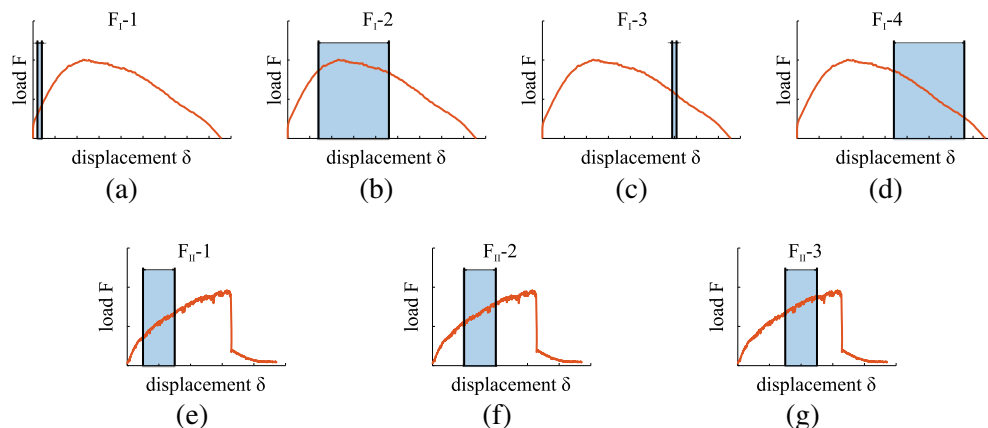


**Fig. 3.** Fatigue testing regimes for (a–d) mode I and (e–g) mode II. (For interpretation of the references to colour in this figure legend, the reader is referred to the web version of this article.)

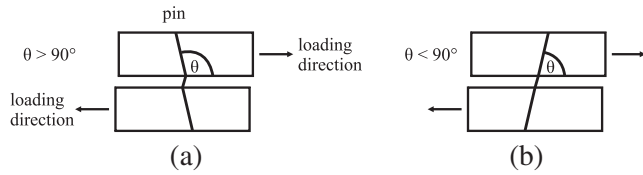


Fig. 4. (a) Loading against and (b) with pin inclination.

**Table 2**  
Averaged properties with standard deviation for quasi-static mode I and mode II tests.

	$P$ in N	$\delta_p$ in mm	$\delta_f$ in mm	$E$ in mJ
Mode I	44	1.2	4.4	120
Standard deviation	6	0.3	0.2	22
Mode II	43	–	0.37	9.8
Standard deviation	6	–	0.09	2.6

$R$  ratios are not used to describe the tests.  $R$  ratios are usually defined by stress levels. As the pin resists both pull-out as well as push-in in mode I this would lead to an effective  $R$  ratio of  $-1$  in the positive displacement regime. In contrast, using lower and upper displacements from testing would give a positive  $R$  ratio.

Fairly low frequencies of 2 and 5 Hz have been chosen to prevent temperature effects. Nevertheless, most configurations have been tested with two different frequencies to highlight any displacement-rate dependent behaviour.

#### 4. Results & discussion

The average quasi-static peak load  $P$ , displacement at  $P$ , i. e.  $\delta_p$ , displacement at final failure  $\delta_f$  and energy dissipation  $E$  for mode I and mode II and the corresponding standard deviation  $\sigma$  are given in Table 2. Due to the brittle material behaviour  $\delta_p$  and  $\delta_f$  are usually very close to each other in mode II. The curves observed do not exhibit a clear load drop associated to initial debonding of the pin from the matrix material, which was present in [28]. However, the ratio of  $\delta_p$  to  $\delta_f$  is about the same. The observed load–displacement curves are similar to those published in [26] for quasi-isotropic layups. The values of  $P$  and  $E$  are slightly higher. This might be due to the different laminate layout.

##### 4.1. Mode I fatigue

###### 4.1.1. General observations

All but two specimens survived the fatigue tests without pin rupture (out of 42 in total). These two specimens are considered

to be outliers. However, one of these is of particular interest, as it failed at a failure load of  $-64$  N during the very first cycles while the test machine was still gradually increasing  $\Delta\delta$  to full scale. It is most likely that buckling caused final failure. Considering the Z-pin as cantilever the critical buckling load  $P_K$  and length  $l_K$ , are related by the EULER formula

$$P_K = \frac{4 * \pi^2 * E_x * I_y}{l_K^2} \quad (1)$$

with modulus of Elasticity along the pin axis  $E_x = 115$  GPa [32], pin diameter  $d = 0.28$  mm and thus second moment of area  $I_y$  given by

$$I_y = \frac{\pi * d^4}{64}. \quad (2)$$

For the pull-out length of  $\delta_f = 4$  mm  $P_K$  is equal to 85.6 N. The average and maximum peak load measured in the quasi-static tests, 44 N and 65 N respectively, result in  $l_K = 5.6$  mm and  $l_K = 4.6$  mm. These theoretical buckling values are far from the experimental ones, particularly in terms of displacement. However, the pin misalignment and the variation in cross sectional pin shape/area are factors contributing to pin breakage due to buckling. This underlines the importance of proper pin manufacture and insertion on one hand. On the other hand, it can be concluded that a stronger bond between the pin and the laminate, as reported for UD-laminates [26] or thicker laminates [33] may cause pin buckling in fatigue. Also, a different pin cross-sectional geometry with a smaller  $I_y$ , as proposed in [34], may cause premature failure when the Z-pins are pushed back into the laminate.

Z-pins pulled out from the top or bottom half of the specimen with no clear preference for either of the two cases. As indicated in Table 2,  $\delta_f > 4$  mm was observed for nearly all specimens, despite the nominal specimen thickness of 8 mm. Typically  $\delta_f$  ranged from 4.0 to 4.7 mm. Zhang et al. [28], who utilised 3 mm thick specimens, reported pull-outs slightly larger than 1.5 mm, too. Here the excess pull-out length in attributed to slightly varying specimen thickness, Z-pin misalignment, as well as small amounts of double sided pull-out.

###### 4.1.2. Fatigue results

Fig. 5a and b gives the change of tensile peak load  $P_F$  and energy dissipation  $E_F$  during the experiments. In all the graphs a very consistent degradation trend can be observed. Hence, sudden failures in either the pin or the laminate (pin splitting, chipping off large surface particles, etc.) did not occur. The average nominal properties at the end of the experiments are given in Table 3 for all configurations. Overall both properties follow the same trend. The degradation is dominated by the effect of  $\Delta\delta$ . These trends did

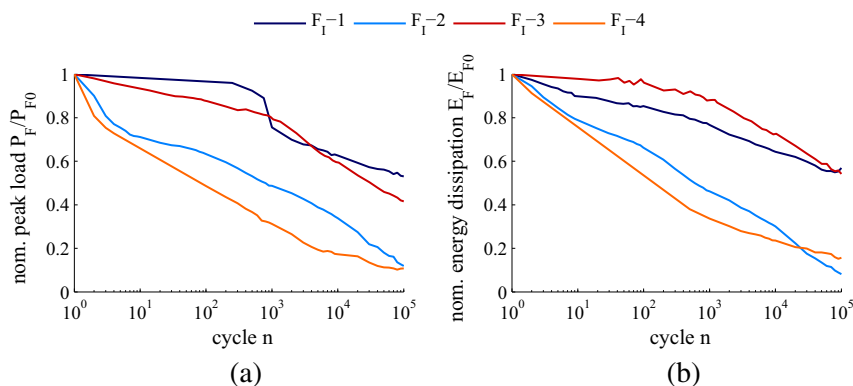
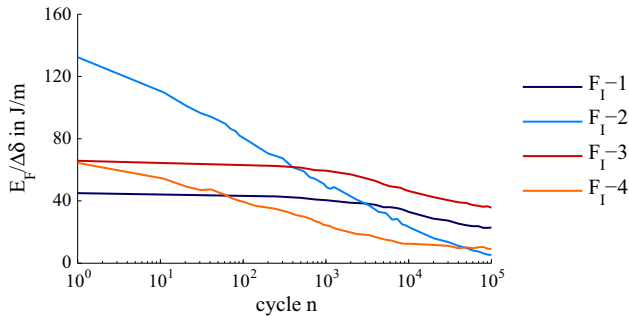


Fig. 5. Representative trend curves of (a) nominal peak load and (b) energy dissipation. (For interpretation of the references to colour in this figure legend, the reader is referred to the web version of this article.)



**Table 3**Nominal properties after  $10^5$  and  $10^6$  cycles.

	$F_{I-1}$	$F_{I-1-1}$	$F_{I-2}$	$F_{I-2-1}$	$F_{I-3}$	$F_{I-4}$
$P_F/P_{F0}$	0.60	0.53	0.11	0.07	0.43	0.12
$E_F/E_{F0}$	0.57	0.55	0.08	0.05	0.47	0.15

**Fig. 6.** Representative curves of  $E_F$  with each cycle normalised by  $\Delta\delta$ . (For interpretation of the references to colour in this figure legend, the reader is referred to the web version of this article.)

not show any significant change for the specimens tested up to  $n = 10^6$ .

The general curve shape differs slightly between the configurations tested with a different  $\Delta\delta$ . A kink can be seen for  $F_{I-1}$  and  $F_{I-3}$  at  $n \approx 10^3$  cycles, similar to what was reported by Zhang et al. [28], whereas the other two configurations show a power law degradation.

More energy is dissipated per cycle for  $F_{I-2}$  and  $F_{I-4}$  throughout the experiment. However, when relating  $E_F$  to  $\Delta\delta$  (Fig. 6), it becomes obvious that this is merely caused by the larger displacements.  $F_{I-1}$  and  $F_{I-3}$  show different trends. This underlines the significance of  $\delta_0$ . Hence, even a nearly pulled-out pin may provide a non-negligible  $E_F$  after a large number of fatigue cycles.

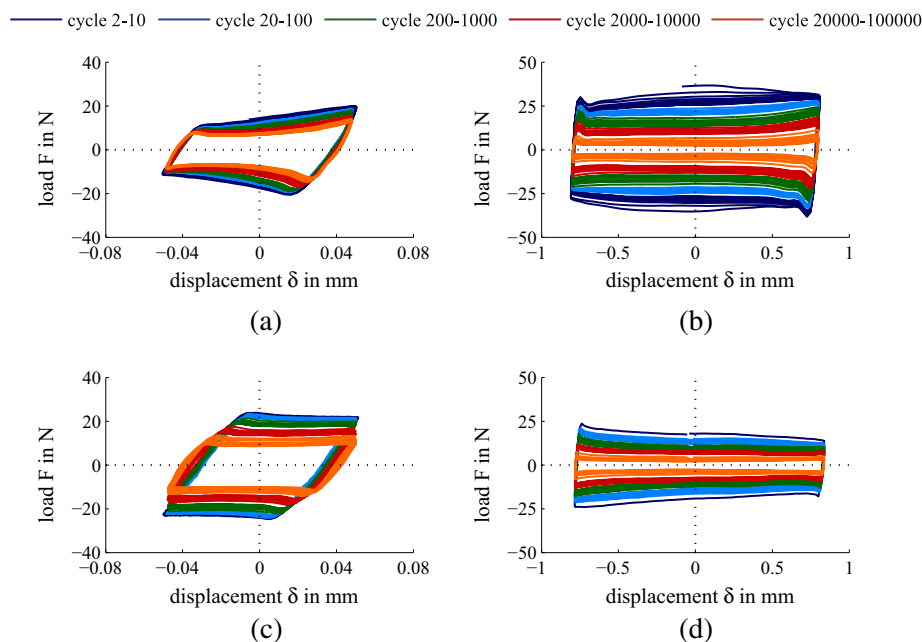
$E_F$  has been measured calculating the hysteresis loop areas. Typical hysteresis curves obtained from the different test configurations are shown in Fig. 7a–d. Coulomb dominated friction is

apparent. Depending on the combination of  $\delta_0$  and  $\Delta\delta$ , the cycles at the start of the test show either the transitions from static to sliding friction only or, alternatively they match the load curve that would be expected in a quasi-static pull-out (e.g.  $F_{I-2}$  gives again the quasi-static peak). For the frequencies examined in this work, no significant displacement rate dependence could be highlighted. The hysteresis shapes at  $n = 10^6$  were virtually identical to those at  $n = 10^5$ .

After fatigue testing, the specimens were quasi-statically loaded until complete pull-out. Fig. 8 shows the full set of pull-out curves obtained from the tests. The dotted grey lines define the band of the load–displacement curves measured in the quasi-static reference tests. Fig. 8a and b was tested with very small average displacements ( $\delta_0 = 0.15$  mm) and amplitude ( $\Delta\delta = 0.05$  mm). Restarted curves are thus very close to the y-axis.

Despite the degradation reported previously, there is no remarkable effect on the residual properties in the configurations cycled with  $\Delta\delta = 0.05$  mm (a, b, e). After restarting the pull-out in a quasi-static regime, these samples initially responded with relatively low loads. After only small amounts of displacement however, a load–displacement trend matching the quasi-static references is recovered. This is also true for  $n = 10^6$  (b). In contrast, a noticeable degradation of residual strength  $P_r$  and residual energy dissipation  $E_r$  can be observed for the specimens cycled with  $\Delta\delta = 0.8$  mm (c, d, f). This degradation increases with  $n$  (d). After the post-fatigue pull-out displacement exceeds the upper displacement level during fatigue  $\delta_u = \delta_0 + \Delta\delta$ , these curves experience some recovery as well. The quasi-static load levels are never fully recovered, though. No noticeable difference between  $f = 2$  Hz and  $f = 5$  Hz on the residual pull-out properties was discerned. The nominal properties of  $P_r$  and  $E_r$  in the restarted tests are given in Table 4. Both of these are determined by comparing the measured pull-out properties to what has been recorded in quasi-static tests within the same displacements ranges ( $\delta_0$  to  $\delta_f$ , respectively). For the specimens cycling with  $\delta_0 < \delta_p$  no significant shift of  $\delta_p$  has been measured.

Zhang et al. [28] reported that cycling before reaching  $P$  had no remarkable influence on the frictional pull-out forces as well. However, as the pull-out curves presented here differ significantly from

**Fig. 7.** Representative hysteresis curves of (a)  $F_{I-1}$ , (b)  $F_{I-2}$ , (c)  $F_{I-3}$  and (d)  $F_{I-4}$ . (For interpretation of the references to colour in this figure legend, the reader is referred to the web version of this article.)

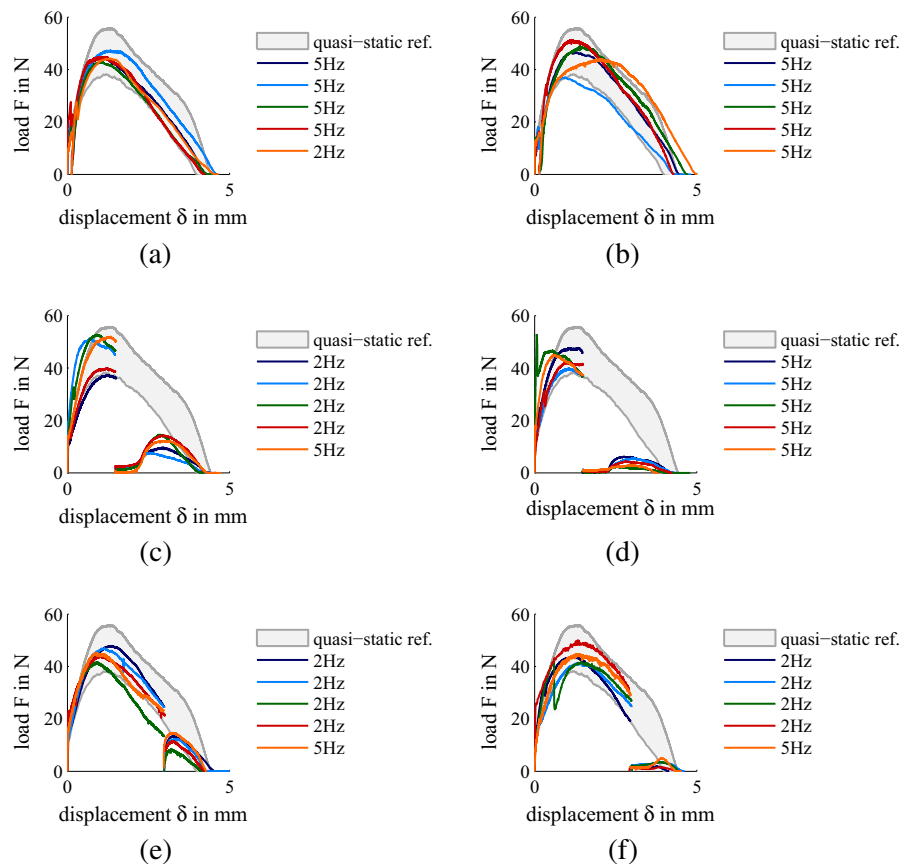


**Fig. 8.** Complete pull-out curves (combined curves of average displacement and residual pull-out, interrupted by fatigue (1)) for (a)  $F_I$ -1, (b)  $F_I$ -1-1, (c)  $F_I$ -2, (d)  $F_I$ -2-1, (e)  $F_I$ -3, (f)  $F_I$ -4. (For interpretation of the references to colour in this figure legend, the reader is referred to the web version of this article.)

**Table 4**

Mode I residual properties (normalised by non-fatigue results) measured in the quasi-static tests after  $10^5$  and  $10^6$  cycles with standard deviation.

	$F_I$ -1	$F_I$ -1-1	$F_I$ -2	$F_I$ -2-1	$F_I$ -3	$F_I$ -4
$P_{rnom}$	1.02	1.03	0.28	0.07	0.57	0.11
Standard deviation	0.15	0.11	0.06	0.03	0.05	0.04
$E_{rnom}$	0.98	0.99	0.24	0.05	0.65	0.16
Standard deviation	0.01	0.0	0.05	0.03	0.18	0.06

those in [28] it is important to investigate the different mechanisms that could cause this behaviour.

A SEM-analysis has been undertaken to explain the observed fatigue and post-fatigue behaviour. Fig. 9 shows SEM images of pulled-out Z-pins. The image of the pin loaded until failure without fatigue (Fig. 9a) shows an uneven, relatively rough surface. The pin diameter matches its nominal value. Resin debris can be seen, the amount of which increases from the pin root to the tip, indicating frictional damage of the composite matrix. There is no significant wear of the fibres.

The surface of the pins cycled with  $\Delta\delta = 0.05$  mm (Fig. 9b) does not exhibit any variation of morphology. This is also true for  $\delta_0 = 0.15$  mm,  $n = 10^5$  and  $n = 10^6$ . The amount of missing fibres and the extent of small damage areas appear to be similar. No significant change in pin diameter was measured. The SEM images presented by Zhang et al. [28] show similar surfaces for the fatigued pins. However, the surface of Z-pins tested under quasi-static loading is covered with a noticeable resin layer.

In contrast, a significant loss of fibres can be seen in the fatigued section of the pins cycled with  $\Delta\delta = 0.8$  mm for  $n = 10^5$  (Fig. 9c). This leads to a slight reduction in pin diameter of about

0.01 mm. However, a relatively rough surface can still be observed. The fibre loss is related to  $n$ . Cycling with  $n = 10^6$  (Fig. 9d) leads to a significantly larger decrease in pin diameter (from 0.28 mm to 0.25 mm) and a substantially smoother surface, reducing friction. The damage is not evenly distributed around the pin. A significant fibre loss can also be observed in the SEM images presented by Pegorin et al. [30] for the pins fatigued in mode I.

The SEM images presented by Schön [35] for frictionally eroded composite surfaces resemble the ones reported here. The same wear mechanisms – matrix gradually worn away and fibres broken off – are described in [35].

The residual pull-out curves (Fig. 8) suggest the onset of localised damage during fatigue. For all the testing regimes considered the load curves show a clear recovery for displacements larger than  $\delta_u$ . However, localised damage is not apparent in the SEM images. Although damage is not distributed evenly around the pin, clearly the presence of surface wear is noticeable along the whole Z-pin segment that experienced alternated sliding. It is possible that the slightly irregular pin pattern causes localised imprints on the pin/laminate interface. When further pull-out occurs the two surfaces do not fit equally well, thus increasing friction.

#### 4.2. Mode II

44 specimens were tested in mode II, 15 of these with  $\delta_0 = 0.1$  mm, 26 with  $\delta_0 = 0.15$  mm and 3 with  $\delta_0 = 0.2$  mm. All specimens were cycled with  $\Delta\delta = 0.05$  mm. For the two first configurations nearly all specimens reached the targeted number of cycles without pin rupture. The few samples failing in fatigue are considered to be outliers. In contrast all 3 specimens tested with

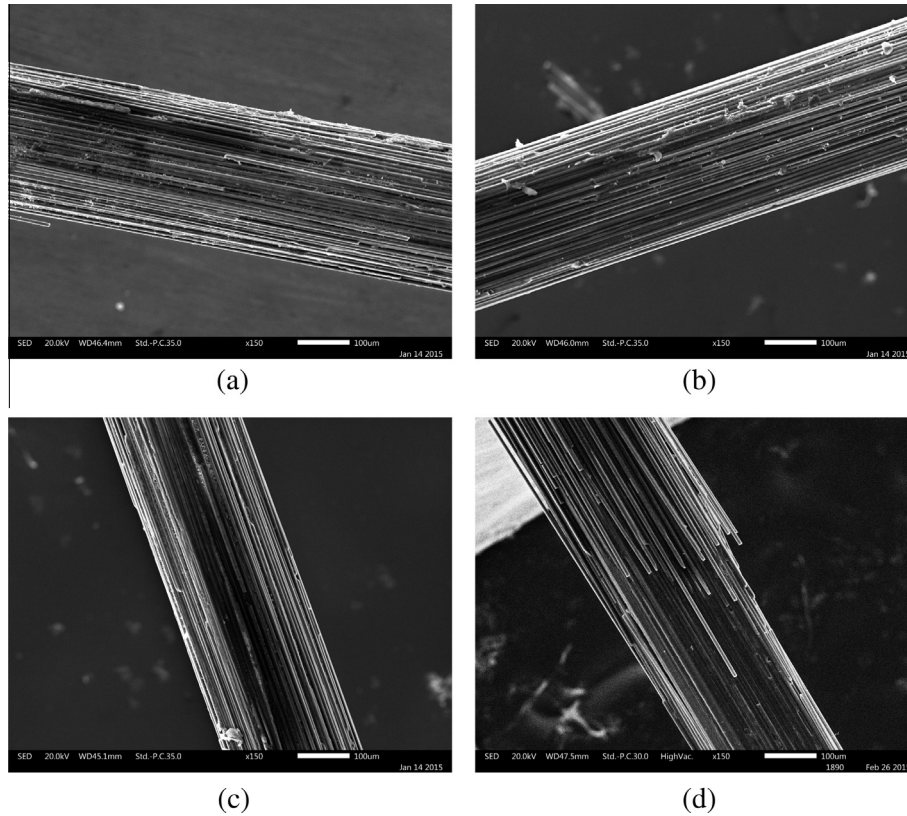


**Fig. 9.** (a) Purely quasi-statically loaded reference and fatigued surface section of pins after cycling with (b)  $\delta_0 = 3.0$  mm,  $\Delta\delta = 0.05$  mm and  $n = 10^5$ , (c)  $\delta_0 = 3.0$  mm,  $\Delta\delta = 0.8$  mm and  $n = 10^5$ , (d)  $\delta_0 = 1.5$  mm,  $\Delta\delta = 0.8$  mm and  $n = 10^6$ .

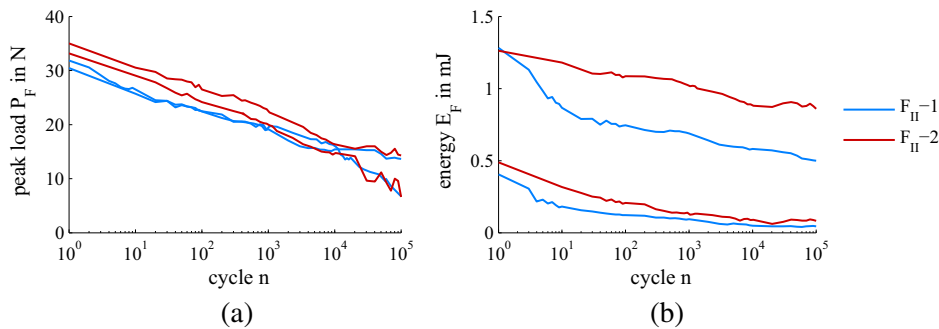


**Fig. 10.** Scatter in (a)  $P_F$  and (b)  $E_F$  for  $F_{II-1}$  and  $F_{II-2}$ . (For interpretation of the references to colour in this figure legend, the reader is referred to the web version of this article.)

$\delta_0 = 0.2$  mm broke during the first cycles while ramping up to full  $\Delta\delta$ .

Trends for both testing regimes did not differ significantly which is partly caused by the relatively high amounts of scatter (Fig. 10). For  $P_F$  a relatively uniform trend was found for the first  $10^4$  cycles. However, scatter increases for further cycles. The degradations of  $P_F$  and  $E_F$  did not correlate as well as for mode I. On average  $E_F$  degrades slightly faster.

As for trends the hysteresis curves for the different testing regimes are similar (Fig. 11). However, some of the hysteresis shapes differ significantly from the ones presented here. Most of the hysteresis curves show a distinct non-linearity within each cycle. The onset of loading is shifted towards larger displacements with greater  $n$ , indicating a softening of the pin foundation. When cycling with  $\Delta\delta = 0.05$  mm and a  $\delta_0 < 0.2$  mm  $E_F$  is about 200–250% higher in mode I than in mode II. As for mode I results, a

change of frequency has no remarkable effect compared to the fatigue induced degradation.

After fatigue cycling the specimens were quasi-statically tested to failure in mode I and “mode II”. For “mode II”, no substantial differences between quasi-static only and post-fatigued specimens cycled with  $\delta_u = 0.15$  mm were found either for  $n = 10^5$  or for  $n = 5 \cdot 10^5$  (Fig. 12a and b). In contrast, some degradation of residual shear properties can be seen for the configurations cycling with  $\delta_u = 0.2$  mm (Fig. 12c and d). As in the mode I tests, the initial loads are substantially lower after restarting the quasi-static shear test, but quickly recover with further displacement. Table 5 shows the degradation of  $P$ ,  $E$  and  $\delta_f$  for the different fatigue regimes. Again, a measure of the degradation was obtained by normalising the residual properties by the corresponding measurements from the reference quasi-static tests without fatigue. In the post-shear-fatigue mode I tests, all but one  $F_{II-2}$  specimen could be



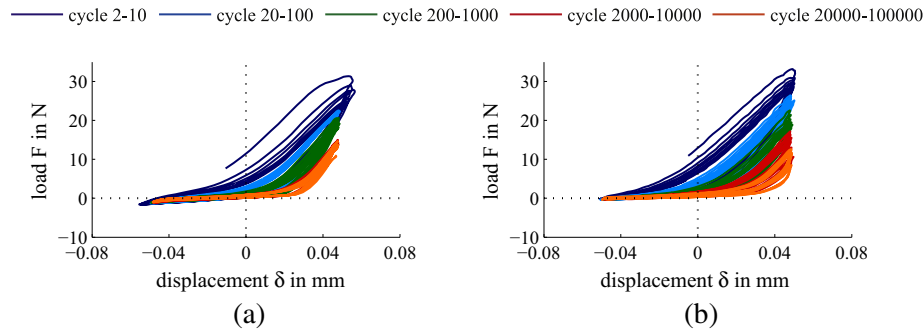


**Fig. 11.** Scatter in (a)  $P_F$  and (b)  $E_F$  for  $F_{II-1}$  and  $F_{II-2}$ . (For interpretation of the references to colour in this figure legend, the reader is referred to the web version of this article.)

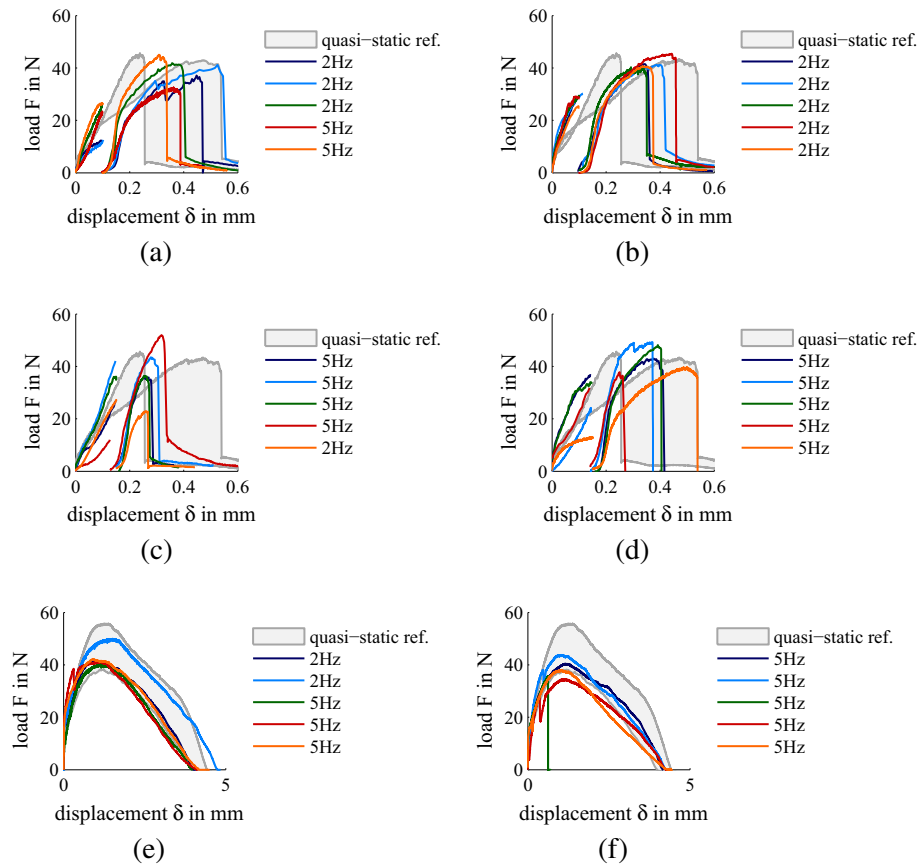


**Fig. 12.** Complete residual test curves in shear (interrupted by fatigue) for (a)  $F_{II-1}$ , (b)  $F_{II-1-1}$ , (c)  $F_{II-2}$  and (d)  $F_{II-2-1}$  & pull out (after shear fatigue) for (e)  $F_{II-1}$  and (f)  $F_{II-2}$ . (For interpretation of the references to colour in this figure legend, the reader is referred to the web version of this article.)

loaded until complete pull-out (Fig. 12e and f). Most curves are relatively close to minimum load levels measured in the quasi-static reference tests. Again, residual properties of the specimen cycling with a larger  $\delta_u$  are slightly lower.

SEM images show two different fracture planes for most pins (Fig. 13). However, this characteristic was present in all configurations tested, including the quasi-static reference tests. This characteristic can also be seen in the specimens tested in mode I after “mode II” fatigue (Fig. 14) and does probably cause the lower mode I residual properties by reducing the pin stiffness. If the fractured area is large enough this may even cause pin rupture in mode I. It is reasonable to assume that the fracture is caused by exceeding certain displacement levels. However, it does not seem to grow significantly during fatigue. Although a load reduction was observed

**Table 5**

Mode II residual properties (normalised by non-fatigue results) measured in the quasi-static after  $10^5$  and  $5 \times 10^5$  cycles with standard deviation.

	$F_{II-1}$	$F_{II-1-1}$	$F_{II-2}$	$F_{II-2-1}$
$P_{nom}$	0.94	0.97	0.91	0.98
Standard deviation	0.10	0.04	0.24	0.17
$E_{nom}$	1.02	0.97	0.55	0.89
Standard deviation	0.25	0.18	0.3	0.39
$\delta_{nom}$	1.17	1.07	0.85	1.04
Standard deviation	0.21	0.11	0.11	0.23

in the hysteresis curves, for both sets of  $\delta_0$  and  $\Delta\delta$  tested successfully in fatigue the specimens running with  $n = 10^5$  and  $n = 5 \times 10^5$  show comparable properties (within scatter) in the residual tests.

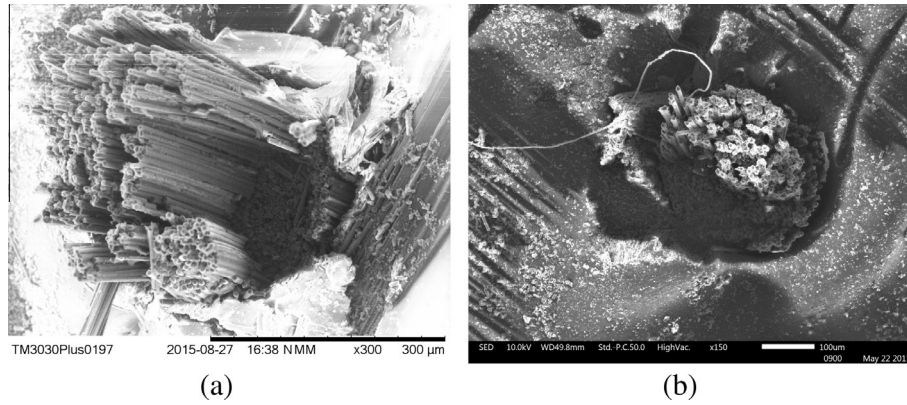


**Fig. 13.** Two different fracture planes in sheared of (a) quasi-static reference and (b)  $F_{II}$ -2 specimens.

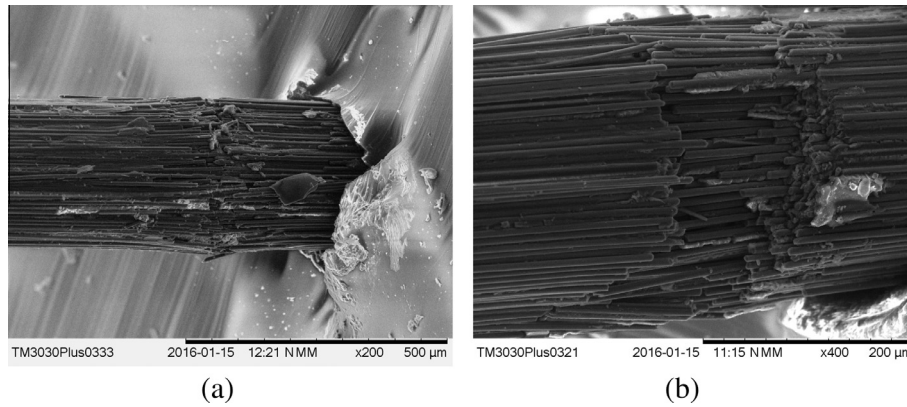


**Fig. 14.** Shear induced damage at the pin root for specimens of configuration (a)  $F_{II}$ -1 and (b)  $F_{II}$ -2.

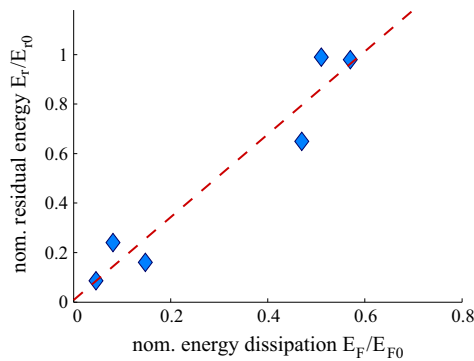


**Fig. 15.** Link between degradation of  $E_F$  and  $E_r$ . (For interpretation of the references to colour in this figure legend, the reader is referred to the web version of this article.)

In contrast, a further increase of  $\delta_u$  to 0.25 mm caused the specimens to fail during the first cycles. The pin performance in mode II fatigue seems to be dominated by  $\delta_u$ .

## 5. Analysis

The mode I results allow the development of a phenomenological model to describe the degradation of energy dissipation per cycle  $D_{E_F}$  and link it to the reduction of residual energy during pull-out  $D_{E_r}$ . The model only accounts for pin displacements within the pull-out region but not for the complete pin pull-out and rein-

section. For mode II no modelling has been undertaken so far, as the results do not allow to distinguish between the different testing regimes trialled.

Using the results from Tables 3 and 4 the nominal energy dissipation per cycle  $\frac{E_F}{E_{F0}}$  is linearly correlated with the nominal of residual energy during pull-out  $\frac{E_r}{E_{F0}}$  (Fig. 15).

The experimentally obtained curve is

$$\frac{E_r}{E_{F0}} = a * \frac{E_F}{E_{F0}} \quad (3)$$

with  $a = 1.7$ . The reduction of  $E_F$  can be expressed via a power law

$$D_{E_F} = 1 - n^{-k} \quad (4)$$

with number of cycles  $n$  and the experimentally determined exponent  $k$ . Eq. (4) matches the experiment curves very well after  $5 * 10^4$  cycles but overestimates the degradation for smaller  $n$  values for some of the fatigue regimes considered (Fig. 5). The  $k$  values obtained are given in Table 6.

According to the experimental results  $k$  only depends on  $\delta_0$  and  $\Delta\delta$ . It is here postulated that

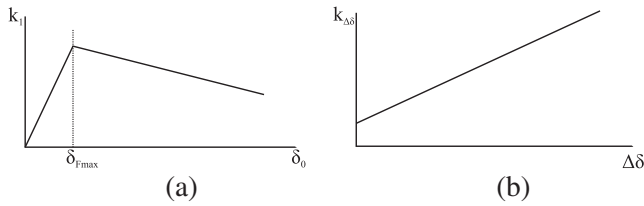
$$k = k_{\delta_0} + k_{\Delta\delta}. \quad (5)$$

Fig. 16 illustrates the assumed general shape of the influence of  $\delta_0$  and  $\Delta\delta$  on  $k$ .

A clear increase of degradation with rising  $\Delta\delta$  was obvious in the experiments. In contrast the influence of  $\delta_0$  follows the quasi-static load curve and depends on the displacement  $\delta_p$  at which the peak load has been reached. The results indicate that the initially higher loads lead to a faster nominal degradation

**Table 6**  
Experimentally obtained  $k$ -factor to model  $D_{Ef}$ .

	$F_I-1$	$F_I-2$	$F_I-3$	$F_I-4$
$k$	0.049	0.221	0.064	0.169



**Fig. 16.** Assumptions for the influence of (a)  $\delta_0$  and (b)  $\Delta\delta$  on degradation exponent.

**Table 7**  
Slopes and constants for the determination of  $k$  based on  $\delta_0$  and  $\Delta\delta$ .

$m_{\Delta\delta}$	$c_{\Delta\delta}$	$m_{1\delta_0}$	$m_{2\delta_0}$	$c_{\delta_0}$
$0.140 \text{ mm}^{-1}$	0.031	$0.074 \text{ mm}^{-1}$	$-0.035 \text{ mm}^{-1}$	0.13

(Table 4). Assuming piece-wise linear interpolations for the exponents lead to:

$$k_{\Delta\delta} = m_{\Delta\delta} * \Delta\delta + c_{\Delta\delta}, \quad (6)$$

$$k_{\delta_0} = m_{1\delta_0} * \delta_0, \quad \text{for } \delta_0 \leq \delta_p, \quad (7)$$

and

$$k_{\delta_0} = m_{2\delta_0} * \delta_0 + c_{\delta_0}, \quad \text{for } \delta_0 > \delta_p \quad (8)$$

with corresponding slopes  $m_{\Delta\delta}$ ,  $m_{1\delta_0}$  and  $m_{2\delta_0}$  and constants  $c_{\Delta\delta}$  and  $c_{\delta_0}$ .

The results obtained allow to set up an under-determined system of equations. By approximating  $k_{\delta_0}(0.15) = 0$  the system can be solved iteratively. The found values for slope and constants after 10 steps are given in Table 7.

This phenomenological model solution allows assessing the nominal energy dissipation caused by the pins during fatigue and residual pull-out based on  $\Delta\delta$  and  $\delta_0$ . The energy dissipation for the first cycle can be estimated on the basis of these parameters, as it has been shown that the tensile load follows the quasi-static loading curve initially and is simply mirrored in the compressive load regime.

## 6. Conclusion

A comprehensive study on micro scale testing of single Z-pins in fatigue has been undertaken. The influence of frequency  $f$ , average displacement  $\delta_0$ , amplitude  $\Delta\delta$  and number of cycles  $n$  on the fatigue and post-fatigue properties in mode I and mode II has been investigated.

In mode I a continuous degradation of  $P_F$  and  $E_F$  without sudden failure was observed. In contrast to other TTR methods like stitching or tufting, large displacements could be tolerated. However, compressive Z-pin failure due to kinking may become an issue for different lay-ups, modified pin geometries or thicker laminates.  $D_{Ef}$  and  $D_{Er}$  are linked nearly linearly. The degradation is substantially affected by  $\Delta\delta$  and, to a lesser extent, by  $\delta_0$ , while the effect of  $f$  is negligible.  $\Delta\delta = 0.05 \text{ mm}$  causes a  $D_{Ef}$  of 40–60% within  $10^5$  cycles and about another 10% for  $10^6$  cycles.  $E_r$  is reduced by 1–35%, depending on  $\delta_0$ . Although  $E_F$  is initially high for large  $\Delta\delta$ , a 90% reduction of  $E_F$  and a 75% drop of  $E_r$  within  $10^5$  cycles was

measured for  $\Delta\delta = 0.8 \text{ mm}$ . The degradation is caused by Z-pin surface erosion and a decrease in friction between the pin and the laminate. No fatigued induced surface damage was observed on the pins cycling with the  $\Delta\delta = 0.05 \text{ mm}$ .

In conclusion small amplitude vibrations can be tolerated by Z-pins for a very high number of cycles. The difference in energy dissipation for Z-pins cycled at small and large displacements is moderate after  $n = 5 * 10^4$ . Thus, Z-pins contribute significantly to fracture resistance by either providing substantial  $E_F$  for a limited number of cycles or moderate  $E_F$  for a very large number of cycles.

A phenomenological model representing the Z-pin energy dissipation during fatigue and for post-fatigue quasi-static loading has been proposed.

Due to Z-pin brittleness in mode II, only very small amplitudes ( $\Delta\delta = 0.05 \text{ mm}$ ) could be tested. Again, a continuous degradation of bridging performance took place during the experiment. However, due to the large scatter no distinct differences among the fatigue scenarios considered could be determined. As long as a critical  $\delta_u$ ,  $\delta_{uK}$  is not exceeded during testing, the reduction of residual properties is limited, although  $E_F$  may be reduced by up to 70%. In contrast, a further increase of  $\delta_u$  leads to Z-pin rupture during the very first cycles. This is caused by fracture at the pin root, whose growth seems to be governed by the applied shear displacement. The effect of ‘mode II’ fatigue on the residual mode I properties is small as long as the decrease of the Z-pin area does not cause the mode I loads to exceed the pin strength.

The overall behaviour of ‘mode II’ fatigue seems to be similar to mode I, e.g. a recovery of Z-pin performance can be observed after  $\delta_u$  is passed, independent from  $n$ . However, the brittle behaviour of Z-pins does only allow for very small amount of shear displacement applied before Z-pin failure.

## Acknowledgements

The authors would like to acknowledge Rolls-Royce Plc and the EPSRC for their support of this research through the Composites University Technology Centre (UTC) at the University of Bristol and Grant No. EP/L505365/1 respectively. Equipment funded by EPSRC under Grant “Atoms to Applications” Grant Ref. EP/K035746/1 was utilised for obtaining the SEM images. Access to supporting data may be requested from Prof. S.R. Hallett, which due to commercial contracts in place, will be subject to consent being granted from the original project participants.

## References

- [1] Marsh G. Airbus A350 XWB update. *Reinf Plast* 2010;54:20–4. [http://dx.doi.org/10.1016/S0034-3617\(10\)70212-5](http://dx.doi.org/10.1016/S0034-3617(10)70212-5).
- [2] Lukaszewicz DH-JA, Ward C, Potter KD. The engineering aspects of automated prepreg layup: history, present and future. *Compos Part B Eng* 2012;43:997–1009. <http://dx.doi.org/10.1016/j.compositesb.2011.12.003>.
- [3] Hufenbach W, Ibrahim FM, Langkamp A, Böhm R, Hornig A. Charpy impact tests on composite structures – an experimental and numerical investigation. *Compos Sci Technol* 2008;68:2391–400. <http://dx.doi.org/10.1016/j.compscitech.2007.10.008>.
- [4] Knaupp M, Baudach F, Franck J, Scharr G. Impact and post-impact properties of cfpr laminates reinforced with rectangular Z-pins. *Compos Sci Technol* 2013;87:218–23. <http://dx.doi.org/10.1016/j.compscitech.2013.08.018>.
- [5] Gude M, Hufenbach W, Koch I, Protz R. Fatigue failure criteria and degradation rules for composites under multiaxial loadings. *Mech Compos Mater* 2006;42:443–50. <http://dx.doi.org/10.1007/s11029-006-0054-z>.
- [6] Allegri G, Jones MI, Wisnom MR, Hallett SR. A new semi-empirical model for stress ratio effect on mode II fatigue delamination growth. *Compos Part A Appl Sci Manuf* 2011;42:733–40. <http://dx.doi.org/10.1016/j.compositesa.2011.02.013>.
- [7] Zhao N, Rödel H, Herzberg C, Gao S-L, Krzywinski S. Stitched glass/PP composite. Part I: Tensile and impact properties. *Compos Part A Appl Sci Manuf* 2009;40:635–43. <http://dx.doi.org/10.1016/j.compositesa.2009.02.019>.
- [8] Dell'Anno G, Cartié DDR, Partridge IK, Rezai A. Exploring mechanical property balance in tufted carbon fabric/epoxy composites. *Compos Part A Appl Sci Manuf* 2007;38:2366–73. <http://dx.doi.org/10.1016/j.compositesa.2007.06.004>.

- [9] Hufenbach W, Kupfer R, Hornig A. Thermoactivated pinning – a novel joining technique for thermoplastic composites. *Solid State Phenom* 2012;188:176–81. <http://dx.doi.org/10.4028/www.scientific.net/SSP.188.176>.
- [10] Mouritz AP. Review of Z-pinned composite laminates. *Compos Part A Appl Sci Manuf* 2007;38:2383–97. <http://dx.doi.org/10.1016/j.compositesa.2007.08.016>.
- [11] Partridge IK, Cartié DDR. Delamination resistant laminates by Z-Fiber® pinning: Part I manufacture and fracture performance. *Compos Part A Appl Sci Manuf* 2005;36:55–64. <http://dx.doi.org/10.1016/j.compositesa.2004.06.029>.
- [12] Allegri G, Zhang X. On the delamination and debond suppression in structural joints by Z-fibre pinning. *Compos Part A Appl Sci Manuf* 2007;38:1107–15. <http://dx.doi.org/10.1016/j.compositesa.2006.06.013>.
- [13] Cartié DDR, Troulis M, Partridge IK. Delamination of Z-pinned carbon fibre reinforced laminates. *Compos Sci Technol* 2006;66:855–61. <http://dx.doi.org/10.1016/j.compscitech.2004.12.018>.
- [14] Isa MD, Feih S, Mouritz AP. Compression fatigue properties of Z-pinned quasi-isotropic carbon/epoxy laminate with barely visible impact damage. *Compos Struct* 2011;93:2269–76. <http://dx.doi.org/10.1016/j.compstruct.2011.03.015>.
- [15] Cartié DDR, Partridge IK. Delamination behaviour of Z-pinned laminates. In: *Proceedings of the 12th international conference on composite materials*, 5–9 July 1999, Paris.
- [16] Liu H-Y, Yan W, Yu X-Y, Mai Y-W. Experimental study on Z-pinned DCB mode I delamination. *Struct Integr Fract* 2004.
- [17] Dai S-C, Yan W, Liu H-Y, Mai Y-W. Experimental study on Z-pin bridging law by pullout test. *Compos Sci Technol* 2004;64:2451–7. <http://dx.doi.org/10.1016/j.compscitech.2004.04.005>.
- [18] Cartié DDR. Effect of Z-Fibres™ in the delamination behaviour of carbon fibre/epoxy laminates [PhD thesis]. Cranfield University; 2000.
- [19] Cartié DDR, Laffaille J-M, Partridge IK, Brunner AJ. Fatigue delamination behaviour of unidirectional carbon fibre/epoxy laminates reinforced by Z-Fiber® pinning. *Eng Fract Mech* 2009;76:2834–45. <http://dx.doi.org/10.1016/j.engfracmech.2009.07.018>.
- [20] Byrd LW, Birman V. The estimate of the effect of Z-pins on the strain release rate, fracture and fatigue in a composite co-cured Z-pinned double cantilever beam. *Compos Struct* 2005;68:53–63. <http://dx.doi.org/10.1016/j.compstruct.2004.02.014>.
- [21] Heimbs S, Nogueira AC, Hombergmeier E, May M, Wolfrum J. Failure behaviour of composite T-joints with novel metallic arrow-pin reinforcement. *Compos Struct* 2014;110:16–28. <http://dx.doi.org/10.1016/j.compstruct.2013.11.022>.
- [22] Yan W, Liu H-Y, Mai Y-W. Mode II delamination toughness of Z-pinned laminates. *Compos Sci Technol* 2004;64:1937–45. <http://dx.doi.org/10.1016/j.compscitech.2004.02.008>.
- [23] Huang HS, Waas AM. Quasi-static mode II fracture tests and simulations of Z-pinned woven composites. *Eng Fract Mech* 2014;126:155–65. <http://dx.doi.org/10.1016/j.engfracmech.2014.05.002>.
- [24] Pegorin F, Pingkarawat K, Daynes S, Mouritz AP. Mode II interlaminar fatigue properties of Z-pinned carbon fibre reinforced epoxy composites. *Compos Part A Appl Sci Manuf* 2014;67:8–15. <http://dx.doi.org/10.1016/j.compositesa.2014.08.008>.
- [25] Rugg KL, Cox BN, Massabó R. Mixed mode delamination of polymer composite laminates reinforced through the thickness by Z-fibers. *Compos Part A Appl Sci Manuf* 2002;33:177–90. [http://dx.doi.org/10.1016/S1359-835X\(01\)00109-9](http://dx.doi.org/10.1016/S1359-835X(01)00109-9).
- [26] Yasaee M, Lander JK, Allegri G, Hallett SR. Experimental characterisation of mixed mode traction–displacement relationships for a single carbon composite Z-pin. *Compos Sci Technol* 2014;94:123–31. <http://dx.doi.org/10.1016/j.compscitech.2014.02.001>.
- [27] Pegorin F, Pingkarawat K, Daynes S, Mouritz AP. Influence of Z-pin length on the delamination fracture toughness and fatigue resistance of pinned composites. *Compos Part B Eng* 2015;78:298–307. <http://dx.doi.org/10.1016/j.compositesb.2015.03.093>.
- [28] Zhang A-Y, Liu H-Y, Mouritz AP, Mai Y-W. Experimental study and computer simulation on degradation of Z-pin reinforcement under cyclic fatigue. *Compos Part A Appl Sci Manuf* 2008;39:406–14. <http://dx.doi.org/10.1016/j.compositesa.2007.09.006>.
- [29] [http://www.hexcel.com/Resources/DataSheets/Prepreg-Data-Sheets/914\\_eu.pdf](http://www.hexcel.com/Resources/DataSheets/Prepreg-Data-Sheets/914_eu.pdf).
- [30] Pegorin F, Pingkarawat K, Mouritz AP. Comparative study of the mode I and mode II delamination fatigue properties of Z-pinned aircraft composites. *Mater Des* 2015;65:139–46. <http://dx.doi.org/10.1016/j.matdes.2014.08.072>.
- [31] Toral Vazquez J, Castanié B, Barrau J-J, Swiergiel N. Multi-level analysis of low-cost Z-pinned composite joints: Part 1: single Z-pin behaviour. *Compos Part A Appl Sci Manuf* 2011;42:2070–81. <http://dx.doi.org/10.1016/j.compositesa.2011.09.018>.
- [32] Allegri G, Yasaee M, Partridge IK, Hallett SR. A novel model of delamination bridging via Z-pins in composite laminates. *Int J Solids Struct* 2014;51:3314–32. <http://dx.doi.org/10.1016/j.ijsolstr.2014.05.017>.
- [33] Mouritz AP, Koh TM. Re-evaluation of mode I bridging traction modelling for Z-pinned laminates based on experimental analysis. *Compos Part B Eng* 2014;56:797–807. <http://dx.doi.org/10.1016/j.compositesb.2013.09.016>.
- [34] Knaupp M, Scharr G. Manufacturing process and performance of dry carbon fabrics reinforced with rectangular and circular Z-pins. *J Compos Mater* 2014;48:2163–72. <http://dx.doi.org/10.1177/0021998313495070>.
- [35] Schön J. Coefficient of friction and wear of a carbon fiber epoxy matrix composite. *Wear* 2004;257:395–407. <http://dx.doi.org/10.1016/j.wear.2004.01.008>.